ISSN: 0067-2904

Density Distributions and Elastic Electron Scattering Form Factors of Proton-rich ^{8}B, ^{17}F, ^{17}Ne, ^{23}Al and ^{27}P Nuclei

Rafah I. Noori[1*], Arkan R. Ridha[2]
[1]Deprtment of Physics, College of Education Ibn Al Haitham, University of Baghdad, Baghdad, Iraq
[2]Deprtment of Physics, College of Science, University of Baghdad, Baghdad, Iraq

Abstract
In this work, the nuclear density distributions, size radii and elastic electron scattering form factors are calculated for proton-rich ^{8}B, ^{17}F, ^{17}Ne, ^{23}Al and ^{27}P nuclei using the radial wave functions of Woods-Saxon potential. The parameters of such potential for nuclei under study are generated so as to reproduce the experimentally available size radii and binding energies of the last nucleons on the Fermi surface.

Keywords: Proton rich nuclei, halo nuclei, density distributions, size radii, elastic electron scattering form factors

توزيعات الكثافة وعوامل التشكل للاستطارة الالكترونية لنوى ^{8}B و ^{17}F و ^{17}Ne و ^{23}Al و ^{27}P الغنية بالبروتونات

رفاه اسماعيل نوري[1*]، أركان رفعه رضا[2]
[1]قسم الفيزياء، كلية التربية للعلوم الصرفة ابن الهيثم،جامعة بغداد، بغداد، العراق
[2]قسم الفيزياء،كلية العلوم،جامعة بغداد، بغداد، العراق

الخلاصة
في هذا العمل، تم حساب توزيعات الكثافة النووية وانصاف الاقطاروعوامل التشكل للاستطارة الالكترونية المرنة لنوى ^{8}B و ^{17}F و ^{17}Ne و ^{23}Al و ^{27}P الغنية بالبروتونات باستخدام الدول الموجية لجهد ودز–ساكسون. معلمات مثل هذا الجهد للنوى تحت الدراسة تم توليدها بحيث يتم توليد انصاف الاقطار العملية المتوفرة وطاقات الربط للنيوكليونات الاخيرة على سطح فيرمي.

Introduction

The chosen radial wave functions are played a crucial role in understanding the nuclear structure in the aspect of nuclear sizes and radial distributions of nucleons in any nuclear system [1]. The experimental matter density distributions of exotic nuclei are mainly characterized by long tail behavior at large r [2]. Electron scattering and muonic atoms (μ^{-}) are pa owerful tool to probe the charge distributions and radii of stable nulei [3]. Unfortunately, due to very short lifetime of halo nuclei there is no ability to make tthe arget of them; therefore, such nuclei are studied in inverse kinematics [4]. The optical isotope shift provides important information about the very tiny quantities of radioactive nuclei [5]. Experimental matter rms radii are available through nucleus-nucleus scattering in Glauber model [6, 7], besides the proton rms radii can be obtained from charge-changing cross section [8]. The naive radial harmonic-oscillator (HO) wave functions are unable to predict the

*Email: 07710638947rf@gmail.com

long-tail characteristic behavior at large r for density distributions of halo nuclei [9-12]. Modifications are adopted to improve such shortcoming such as using two HO size parameters for core and halo parts to regenerate the asymptotic behavior and size radii but with adequate results [13-15]. The transformed HO wave functions in local-scale transformation opnened new approach to reform the performance of the radial wave functions of halo nuclei in [16-18].The single-particle wave functions of Woods-Saxon (WS) potential are used with very good agreements with experimental data for both stable and exotic nuclei [19-22].

In present work, we undertook the calculation of rms radii, density distributions and elastic electron scattering form factors for proton-rich ^{8}B, ^{17}F, ^{17}Ne, ^{23}Al and ^{27}P nuclei utilizing the realistic radial wave functions of WS potential.

Theoretical formulations

The nuclear transition proton ($t_z = 1/2$)/neutron ($t_z = -1/2$) density distributions can be written as [13]

$$\rho_{J,t_z}(r) = \frac{1}{\sqrt{4\pi(2J_i+1)}} \sum_{aa'} X^{J_i,J_f,J}_{a,a',t_z} \langle j_{a'} || Y_J || j_a \rangle R_{a',t_z}(r) R_{a,t_z}(r) \quad (1)$$

where a and a' denote the single-particle state (nlj). $X^{J_iJ_f,J}_{aa',t_z}$ represents the weight of transition obtained from shell-model calculations. In Eq. (1), the radial wave functions of WS potential $\left(R_{nlj,t_z}(r)\right)$ are taken from the solution to radial part of the Schrodinger equation using Woods-Saxon potential given below [23]

$$\left(\frac{\hbar^2}{2\mu}\frac{d^2}{dr^2} - U(r) - \frac{l(l+1)\hbar^2}{2\mu r^2} \varepsilon_{nlj,t_z}\right) R_{nlj,t_z}(r) = 0 \quad (2)$$

In the above equation, $\mu_{tz} = \frac{m_{tz}(A-1)}{A}$ is the reduced mass of the core $(A-1)$ and single nucleon, m_{tz} is the mass of single nucleon, A is the atomic mass and ε_{nlj,t_z} represents the binding energy of single nucleon in the state nlj. The potential $U(r)$ can be written as

$$U(r) = U_{cent}(r) + U_{s.o.}(r) + U_c(r) \quad (3)$$

The three terms in the Eq. (3), stand for the central, spin-orbit and Coulomb parts, respectively, given by [23]

$$U_{cent}(r) = \frac{-U_0}{\left(1+e^{\left(\frac{r-R}{a}\right)}\right)},$$

$$U_{s.o.}(r) = \left(\frac{\hbar}{m_\pi c}\right)^2 \frac{U_{s.o.}}{r}\frac{d}{dr}\frac{1}{\left(1+e^{\left(\frac{r-R_{s.o.}}{a_{s.o.}}\right)}\right)}\langle \hat{l}.\hat{\sigma}\rangle = -\left(\frac{\hbar}{m_\pi c}\right)^2 \frac{U_{s.o.}}{r}\frac{e^{\left(\frac{r-R_{s.o.}}{a_{s.o.}}\right)}}{\left(1+e^{\left(\frac{r-R_{s.o.}}{a_{s.o}}\right)}\right)^2}\langle \hat{l}.\hat{\sigma}\rangle$$

and

$$U_c(r) = \begin{cases} (Z-1)\frac{e^2}{r} & if\ r > R \\ \frac{(Z-1)e^2}{2R}\left[3 - \frac{r^2}{R^2}\right] & if\ r < R \end{cases} \text{ for protons and } U_c(r) = 0 \text{ for neutrons} \quad \ldots\ldots..(4)$$

In the first and second terms of Eq. (4), U_0, a and $\left(R = r_0(A-1)^{1/3}\right)$ and $U_{s.o.}$, $a_{s.o.}$ and $R_{s.o.}$ $\left(R_{s.o.} = r_{s.o.}(A-1)^{1/3}\right)$ are the depth of central/spin-orbit part, the diffuseness of central/spin-orbit part and radius parameter of central/spin-orbit part. $(m_\pi c^2 = 139.57 MeV)$, $\hbar c = 197.33\ MeV\ fm$ and $\left(\frac{\hbar}{m_\pi c}\right)^2 \approx 2\ fm^2$ (where m_π is the pion mass). The matrix element of $\langle \hat{l}.\hat{\sigma}\rangle$ written in the second term of Eq. (4) is given by

$$\langle \hat{l}.\hat{\sigma}\rangle = \begin{cases} -\frac{1}{2}(l+1) & for\ j = l - \frac{1}{2} \\ \frac{l}{2} & for\ j = l + \frac{1}{2} \end{cases} \quad (5)$$

The last term in Eq. (4), indicates the Coulomb potential generated by a homogeneous charged sphere. Besides, the radial wave functions of HO potential is used in Eq. (1) in order to compare with the results of WS.

The ground point proton/neutron density distribution can be written from Eq. (1) as

$$\rho_{J=0,t_z}(r) = \frac{1}{4\pi}\sqrt{\frac{2j_a+1}{2J_i+1}}\sum_a X_{a,a,t_z}^{J_i,J_i,J=0}\left|R_{nlj,t_z}(r)\right|^2 \quad (6)$$

The total charge density distribution can be calculated from Eq. (6) by folding the point density distributions of protons and neutrons into the charge density of each one separately as follows

$$\rho_{J=0,ch}(r) = \rho_{ch,t_z=1/2}(r) + \rho_{ch,t_{z=-1/2}}(r) \quad (7)$$

in the above equation, the first and second terms can be written as

$$\rho_{ch,t_z=1/2}(r) = \int \rho_{J=0,t_z=1/2}(r)\rho_p(r-r')dr' \quad (8)$$

and

$$\rho_{ch,t_z=-1/2}(r) = \int \rho_{J=0,t_z=-1/2}(r)\rho_n(r-r')dr' \quad (9)$$

$\rho_p(\vec{r})$ [24] and $\rho_n(\vec{r})$ [25] in Eqs. (8) and (9) takes, respectively the following forms

$$\rho_p(r) = \frac{1}{\left(\sqrt{\pi}a_{pr}\right)^3}e^{\left(\frac{-r^2}{a_p^2}\right)} \quad (10)$$

and

$$\rho_n(r) = \frac{1}{\left(\pi r_i^2\right)^{3/2}}\sum_1^2 \theta_i \ \mathrm{e}^{-r^2/r_i^2} \quad (11)$$

The parameters in Eqs. (10) and (11) are taken from Ref. [24] and [25], respectively.
The rms radii of neutrons, protons, charge and matter are calculated from

$$\langle r^2\rangle_i^{1/2} = \sqrt{\frac{4\pi}{i}\int_0^\infty \rho_{J=0,i}(r)r^2dr} \quad (12)$$

where i stands for N (number of neutrons), Z (atomic number), charge and A (mass number), respectively.
Finally, in the first Born approximation, the longitudinal electron scattering form factors can be written as [26, 27]

$$F_{J,ch}^C(q) = \sum_{t_z} F_J^C(q,t_z)\, f_{t_z}(q) \quad (13)$$

where

$$F_J^C(q,t_z) = \frac{1}{z}\sqrt{\frac{4\pi}{(2J_i+1)}}\langle J_f\left\|\boldsymbol{O}_J^C(q,t_z)\right\|J_i\rangle \quad (14)$$

The Coulomb multipole operator in Eq. (14) is given by

$$\boldsymbol{O}_{JMJ}^C(q,t_z) = \int j_J(qr)Y_{JMJ}(\Omega_r)\hat{\rho}_{t_z}(\vec{r}) \quad (15)$$

The many-body matrix element in Eq. (14) can be written in terms of single matrix element as follows [27]

$$\langle J_f\left\|\boldsymbol{O}_J^C(q,t_z)\right\|Ji\rangle = \sum_{aa'} X_{a,a',p/n}^{J_i,J_f,J}\langle a',t_z\left\|O_J^C(q,r,t_z)a,t_z\right\|a,t_z\rangle \quad (16)$$

The single Coulomb multipole opertor is given by

$$O_J^C(q,r,t_z) = e_{t_z}j_J(qr)Y_J(\Omega_r) \quad (17)$$

The Coulomb form factor in Eq. (14) can be simplified to

$$\left|F_{J,ch}^C(q)\right| = \frac{1}{Z}\sqrt{\frac{4\pi}{(2J_i+1)}}\left|\int_0^\infty j_J(qr)\rho_{J,ch}(r)r^2dr\right| \quad (18)$$

For $C0$ component in the above equation can be written as

$$\left|F_{J=0,ch}^C(q)\right| = \frac{1}{Z}\sqrt{\frac{4\pi}{(2J_i+1)}}\left|\int_0^\infty j_0(qr)\rho_{J=0,ch}(r)r^2dr\right| \quad (19)$$

The transition density distribution is calculated from the contribution of core-polarization (CP) and model-space (MS) [27]:

$$\rho_{ch,J}(r) = \rho_{ch,J}^{CP}(r) + \rho_{ch,J}^{MS}(r) \quad (20)$$

In the present work, $\rho_{ch,J}^{CP}(r)$ is calculated using Tassie [27] and Bohr-Mottelson [28] models, respectively.

$$\rho_{ch,J}(r) = Nr^{J-1}\frac{d}{dr}\rho_{ch}(r) \quad (21)$$

and

$$\rho_{ch,J}(r) = N\frac{d}{dr}\rho_{ch}(r) \quad (22)$$

where, N in the above two equations are found so as to reproduce the experimental multipole moments and $\rho_{ch}(r)$ is calculated from Eq. (7).

$\rho^{MS}_{J,ch,t_z}(r)$ is related to the point proton/neutron transition density distributions and calculated from Eq.(1). The incoherent sum of multipole coulomb form factors can be written as

$$|F(q)|^2 = \sum_J \left|F^C_{J,ch}(q)\right|^2 \quad (24)$$

Results and Discussion

The radial wave functions of WS potential are used to calculate the density distributions, rms radii and elastic electron scattering charge form factors for ^{8}B, ^{17}F, ^{17}Ne, ^{23}Al and ^{27}P nuclei. The parameters of WS potential (U_0, r_0, a_0, $r_{s.o.}$ and $a_{s.o.}$) displayed in Table-1 are chosen so as to reproduce the experimental single-nucleon binding energies (for the last proton and neutron on Fermi surface) and available experimental rms radii for nuclei under study. The depth of spin-orbit ($U_{s.o.}$) is fixed to be 9.0 MeV.

In Table-2, the calculated and available experimental rms radii for nulei under study are displyed. It is clear that the experimental data are well generated for the used WS parameters. In Tables-(3-7), the single binding energies of protons and neutrons predicted by the fixed parameters of WS potential are presented for ^{8}B, ^{17}F, ^{17}Ne, ^{23}Al and ^{27}P nuclei. It is obvious that the last single nucleon binding energies for both protons and neutrons are well reproduced.

In Figures-(1,2) the calculated matter density distributions for ^{8}B (a), ^{17}F (b), ^{17}Ne (c), ^{23}Al (d) and ^{27}P (e) are represented by solid and dashed curves for WS and HO, respectively are depicted and compared with experimental data represented by the shaded area. From calculations, it is clear that results of WS are in very good agreement with experimental data for all r especially the tail region on contrary to the results of HO which completely failed to reproduce the tail region due to the Gaussian fall-off behavior of radial wave function at asymptotic region. Knowing that the ^{8}B, ^{23}Al and ^{27}P are 1p- halo, ^{17}F is 1p-skin and ^{17}Ne is 2p-halo [2, 4, 7]. The proton and neutron density distributions for nuclei under study are drawn in Figure-2 for ^{8}B (a), ^{17}F (b), ^{17}Ne (c), ^{23}Al (d) and ^{27}P (e). The long tail characteristic is well generated in the proton distribution denoting the existence of halo in ^{8}B, ^{17}Ne, ^{23}Al and ^{27}P nuclei (due to the low binding energies of the last protons) and skin in ^{17}F.

In Figure-3, the C0 component of the elastic Coulomb electron scattering form factors for exotic ^{8}B (a), ^{17}F (b), ^{17}Ne (c), ^{23}Al (d) and ^{27}P (e) nuclei represented by solid curves and compared with the C0 components of the corresponding stable ^{10}B (a), ^{19}F (b), ^{20}Ne (c), ^{27}Al (d) and ^{31}P (e) nuclei, respectively. For stable nuclei mentioned previously, the CKII interaction [29] with 1p-model space (for ^{10}B) and SDBA interaction [30] with sd-shell model space (^{19}F, ^{20}Ne, ^{27}Al and ^{31}P nuclei) are used. The shell model calculations with the aforementioned two effective interactions are done using OXBASH code [31]. It is clear that the ^{8}B, ^{17}F, ^{17}Ne and ^{27}P nuclei have forward and fluctuated downward shifts while ^{23}Al nuclei has backward and fluctuated downward shifts.

In Figure-4, the calculated charge form factors of stable ^{10}B (a), ^{19}F (b), ^{20}Ne (c), ^{27}Al (d) and ^{31}P (e) nuclei are depicted and compared with those of experimental data. The radial wave functions of WS potential are used to calculate the charge form factors. The C0+C2 and C0+C2+C4 components are calculated for ^{10}B and ^{27}Al while C0 components are calculated for ^{19}F, ^{20}Ne and ^{31}P. The higher CJ components for ^{10}B and ^{27}Al are calculated from the contribution of core-polarization, using Tassie (T) [27] (solid curve) and Bohr-Mottelson (BM) [28] (dashed curve) models, and the model space, using Eq. (1). The CKII [29] and SDBA [30] interactions are used for ^{10}B and ^{19}F, ^{20}Ne, ^{27}Al and ^{31}P, respectively. From the overall figures, there are in general good agreements with experimental data.

Table 1-Woods-Saxon potential Parameters for nuclei under study

$^{A}_{Z}X_{N}$		U_0 (MeV)	r_0 (fm)	a_0 (fm)	$U_{s.o.}$ (MeV)	$r_{s.o.}$ (fm)	$a_{s.o.}$ (fm)
$^{8}_{5}B_3$	Neutrons	58.07	1.35	0.5	9.0	1.35	0.5
	Protons	48.1	1.405	0.42	9.0	1.405	0.42
$^{17}_{9}F_8$	Neutrons	59.750	1.23	0.650	9.0	1.23	0.650
	Protons	55.17	1.19	0.82	9.0	1.40	0,76
$^{17}_{10}Ne_7$	Neutrons	57.690	1.22	0.580	9.0	1.22	0.580
	Protons	53.021	1.331	0.405	9.0	1.33	0.405
$^{23}_{13}AL_{10}$	Neutrons	60.941	1.26	0.350	9.0	1.26	0.350
	Protons	44.574	1.350	0.30	9.0	1.350	0.30
$^{27}_{15}P_{12}$	Neutrons	60.0	1.280	0.581	9.0	1.280	0.581
	Protons	47.423	1.250	0.650	9.0	1.250	0.650

Table 2-The calculated rms radii for nuclei under study

${}^{A}_{Z}X_{N}$	$\langle r_p^2\rangle^{1/2}$ fm	Exp. $\langle r_p^2\rangle^{1/2}$ fm	$\langle r_n^2\rangle^{1/2}$ fm	Exp. $\langle r_n^2\rangle^{1/2}$ fm	$\langle r_{ch}^2\rangle^{1/2}$ fm	Exp. $\langle r_{ch}^2\rangle^{1/2}$ fm	$\langle r_m^2\rangle^{1/2}$ fm	Exp. $\langle r_m^2\rangle^{1/2}$ fm
${}^{8}_{5}B_{3}$	2.806	2.76(8) [32]	2.135	2.16(8)	2.825	2.82(6) [33]	2.575	2.55(8) [32]
${}^{17}_{9}F_{8}$	2.907	2.90±0.15 [34]	2.482	2.478±0.18 [34]	2.995	-	2.715	2.71±0.18 [34]
${}^{17}_{10}Ne_{7}$	3.008	-	2.443		3.063	3.0413 [35]	2.789	2.75(7) [36]
${}^{23}_{13}AL_{10}$	3.136	3.1±0.25 [34]	2.605	2.634±0.23 [34]	3.211	-	2.917	2.905±0.25 [34]
${}^{27}_{15}P_{12}$	3.308	3.22±0.163 [34]	2.836	2.754±0.14 [34]	3.386	-	3.107	3.02±0.155 [34]

Table 3-Single-nucleon binding energies for ^{8}B

state	Single-neutron binding energy (MeV)	Single-proton binding energy (MeV)
$1s_{1/2}$	- 30.119	- 22.048
$1p_{3/2}$	- 12.822	- 7.078
$1p_{1/2}$	- 5.363 [37]	- 0.147 [37]

Table 4-Single-nucleon binding energies for ^{17}F

state	Single-neutron binding energy (MeV)	Single-proton binding energy (MeV)
$1s_{1/2}$	-36.813	-25.27
$1p_{3/2}$	-22.266	-12.422
$1p_{1/2}$	-16.8 [37]	-7.481
$1d_{5/2}$	-	- 0.60 [37]

Table 5-Single-nucleon binding energies for ^{17}Ne

state	Single-neutron binding energy (MeV)	Single-proton binding energy (MeV)
$1s_{1/2}$	-35.786	-31.582
$1p_{3/2}$	-21.252	-19.044
$1p_{1/2}$	-15.557	-14.224
$1d_{5/2}$	-6.837	-5.862
$2s_{1/2}$	-3.822 [37]	- 0.467 [37]

Table 6-Single-nucleon binding energies for ^{23}Al

state	Single-neutron binding energy (MeV)	Single-proton binding energy (MeV)
$1s_{1/2}$	-46.05	-26.860
$1p_{3/2}$	-33.37	-17.134
$1p_{1/2}$	-29.612	-13.692
$1d_{5/2}$	-19.525	- 6.496
$2s_{1/2}$	-12.038	- 0.141 [37]
$1d_{3/2}$	-11.01 [37]	-

Table 7-Single-nucleon binding energies for ^{27}P

state	Single-neutron binding energy (MeV)	Single-proton binding energy (MeV)
$1s_{1/2}$	-44.336	-24.711
$1p_{3/2}$	-32.408	-14.412
$1p_{1/2}$	-28.894	-10.453
$1d_{5/2}$	-19.764 [37]	-3.901
$2s_{1/2}$	-	- 0. 870 [37]

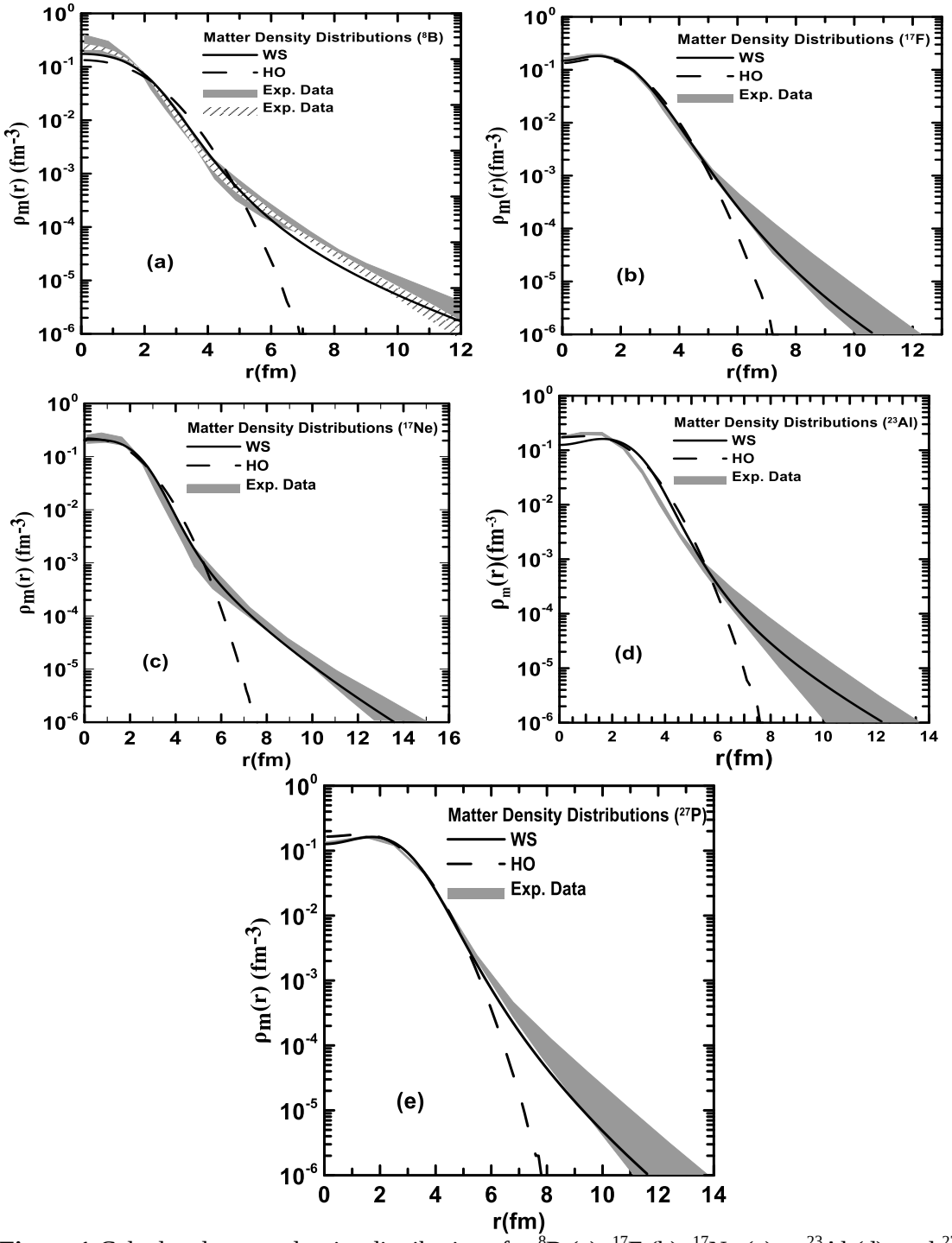

Figure 1-Calculated matter density distributions for ^{8}B (a), ^{17}F (b), ^{17}Ne (c), ^{23}Al (d), and ^{27}P (e).the shaded areas represent experimental data and taken from ^{8}B [38], ^{17}F [34], ^{17}Ne [41], ^{23}Al [34], and ^{27}P [34].

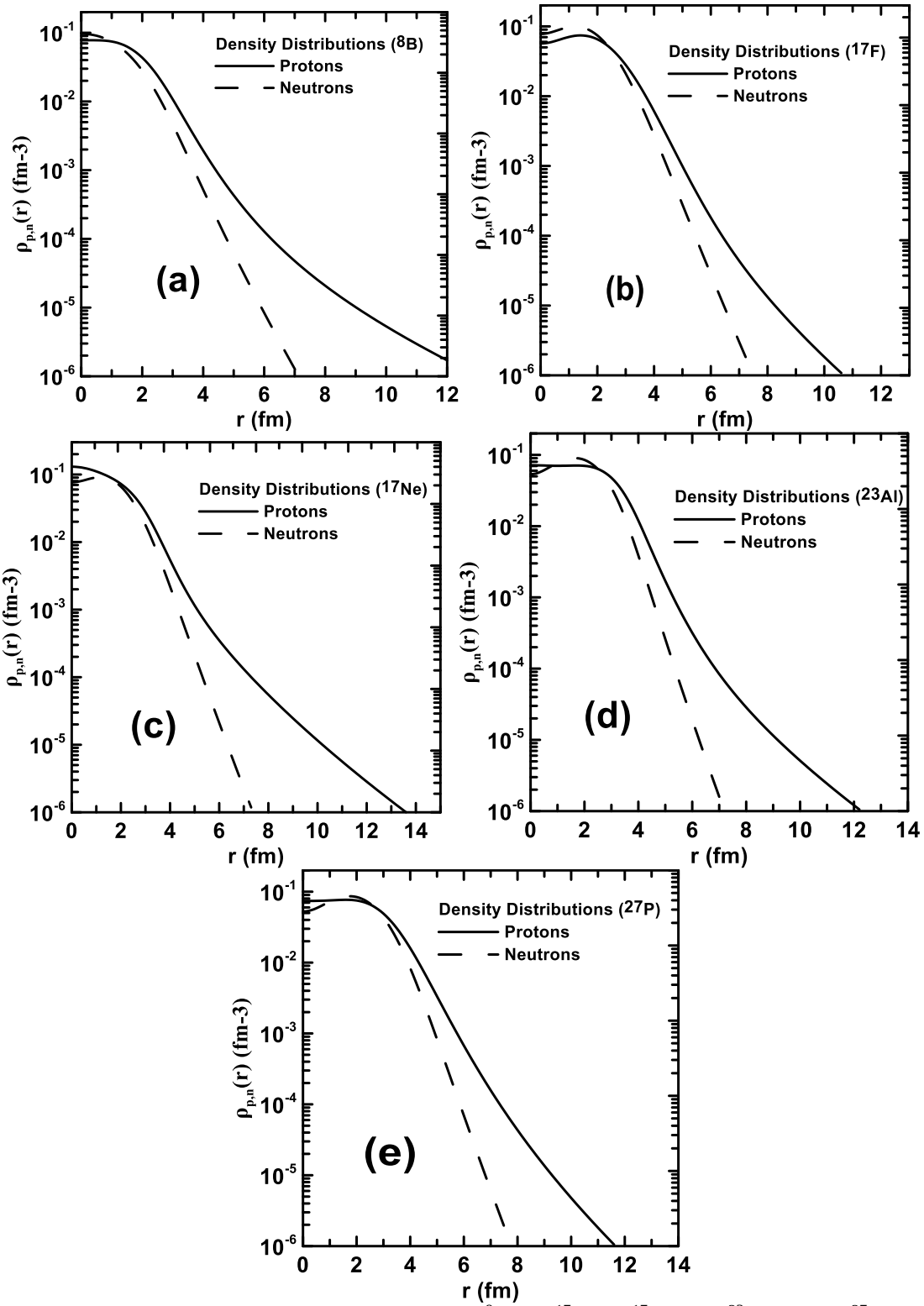

Figure 2-Proton and neutron density distributions for ^{8}B (a), ^{17}F (b), ^{17}Ne (c), ^{23}Al (d) and ^{27}P (e).

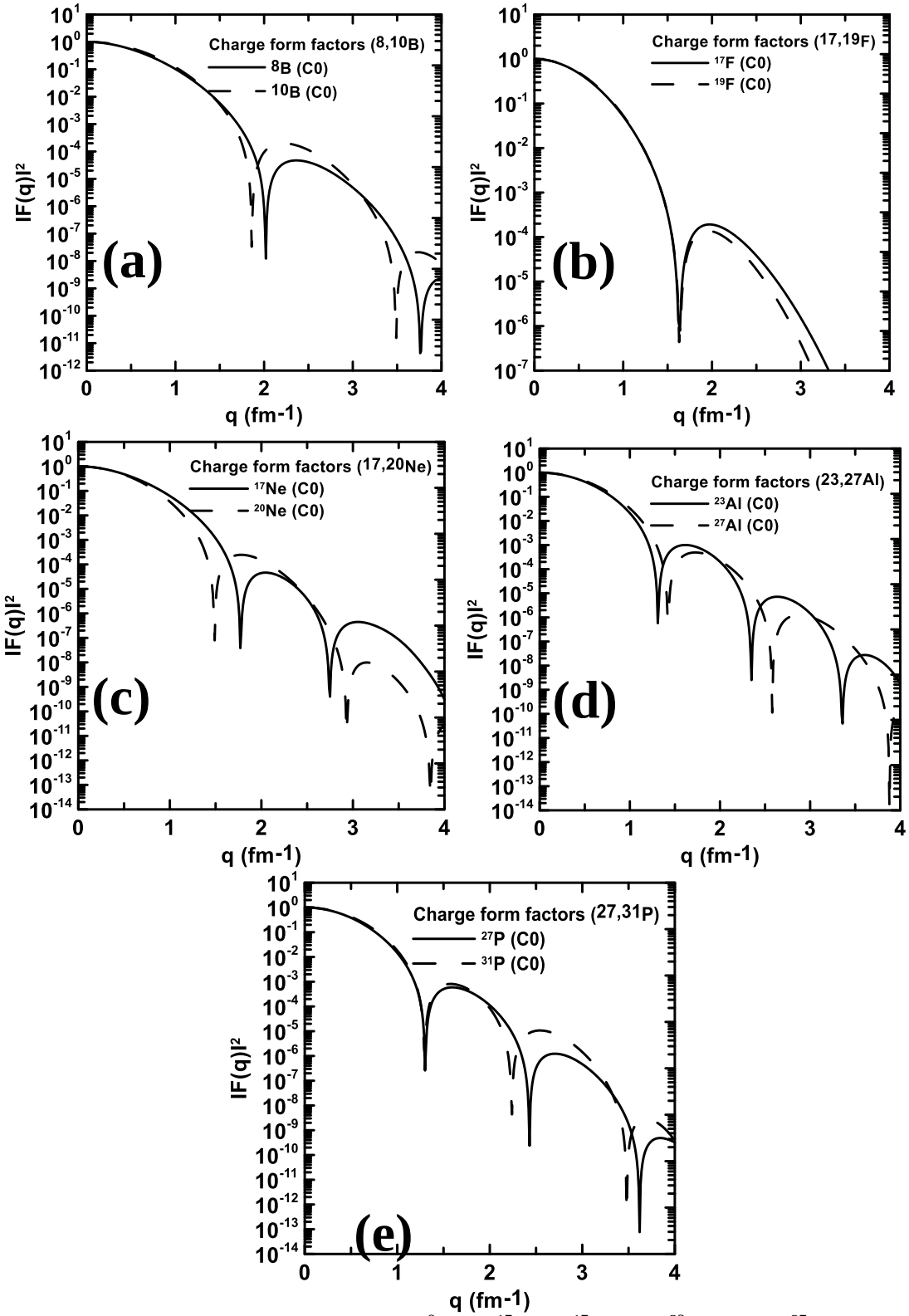

Figure 3-The calculated charge form factors for ^{8}B (a), ^{17}F (b), ^{17}Ne (c), ^{23}Al (d) and ^{27}P (e).

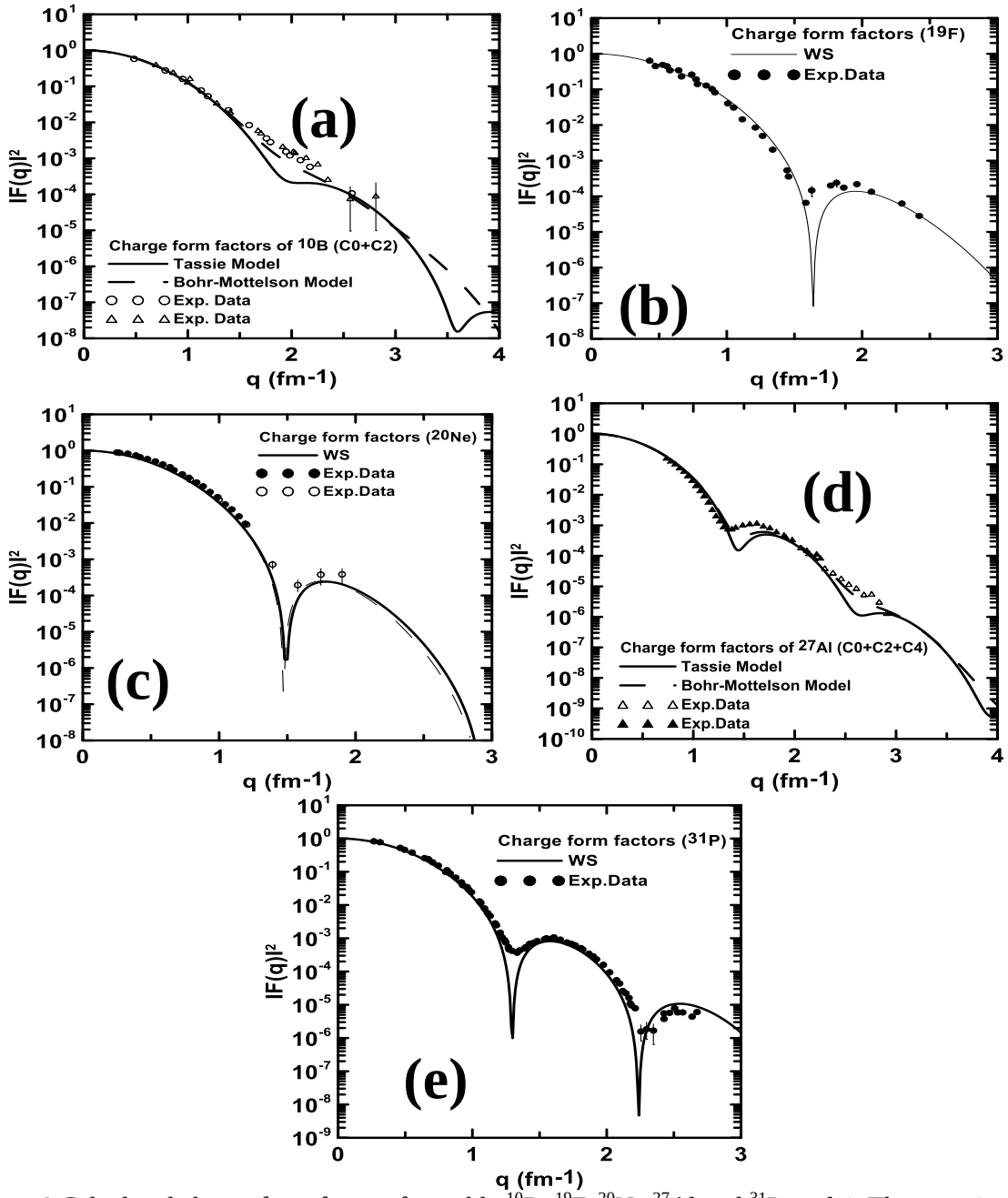

Figure 4-Calculated charge form factors for stable ^{10}B, ^{19}F, ^{20}Ne,^{27}Al and ^{31}P nuclei. The experimental data are presented by empty circles[39], [40], triangles [41] ^{10}B, ^{19}F [42], ^{20}Ne [43], ^{27}Al [44], and ^{31}P [45].

Conclusions

The nuclear density distribution and elastic electron scattering form factors have been calculated using the radial wave functions of WS potential. The parameters of such potential are selected so as to reproduce firstly the binding energy of the single nucleon on the Fermi surface and secondly the available experimental rms radii for proton-rich nuclei under study. For the calculated matter densities, the results are in very good agreement with those of experimental data. It is found a noticeble long tail in ^{8}B, ^{17}Ne, ^{23}Al and ^{27}P indicating the presence of halo and this is attriubuted to the low binding energies of the last proton(s), besides the low orbital quantum numbers where the last proton(s) are found to be in $1p_{1/2}$ for ^{8}B, $2s_{1/2}$ for^{17}Ne, ^{23}Al and ^{27}P while in ^{17}F in spite of very low binding energy of the last proton, it is found a skin behavior due to the existence of such proton in $1d_{5/2}$ (the centrifugal term in effective potential is high pushing the last proton to the core and diminishing the tail). For the calculated charge form factors, the C0 component for ^{19}F, ^{20}Ne and ^{31}P, The C0+C2 component for ^{10}B

and C0+C2+C4 component for ^{27}Al are calculated and compared with available experimental data. The results for exotic nuclei are left for the future projects on electron-radioactive ion beams which proposed to build to study the access of protons or neutrons on charge form factors.

References

1. Batty, C. J., Friedman, E., Gils, H. J. and Rebel, H. **1989**. Experimental methods for studying nuclear density distributions. *Advances in Nuclear Physics*, **19**: 1–188.
2. Tanihata, I., Savajols, H. and Kanungo, R. **2013**. Recent experimental progress in nuclear halo structure studies. *Progress in Particle and Nuclear Physics*, **68**: 215–313.
3. Bohr A. and Mottelson B.R. **1969**. "Nuclear structure / Vol. 1, Single-particle motion", New York [etc.]: Benjamin.
4. Tanihata, I. **1996.** Neutron halo nuclei. *J. Phys G: Nucl. Part Phys*. **22**: 157-198.
5. Otten, W. E. **1987.** *Nuclear Radii and Moments of Unstable Isotope, Treatise of Heavy-Ion Physics*. Vol. **8**, Plenum Press, New York
6. Tanihata, I., Hamagaki, H., Hashimoto, O., Nagamiya, S., Shida, Y., Yoshikawa, N., Yamakawa, O., Sugimoto, K., Kobayashi, T., Greiner, D.E., Takahashi, N. and Nojiri, Y. **1985**. Measurements of interaction cross sections and radii of He isotopes. *Phys. Lett. B*, **160**: 380-384.
7. Ozawa A., Suzuki T., Tanihataa I.**2001**. Nuclear size and related topics. Nuclear Physics A **693**, pp: 32–62. Blank B.,Gaimard J.-J., Geissel H., Schmit K.-H., Stelzer H., Summerer K., Bazin D., Del
8. Moral R., Dufour J. P., Fleury A., Hubert F., Clerc H.-G., Steiner M. **1992**.Charge-changing cross sections of the neutron –rich isotopes ^{8,9,11}Li. Z. *Phys. A*, **343**: 375-379.
9. Navratil, P. and Barrett, B. R. **1996.** No-core shell-model calculations with starting- energy independent multivalued effective interactions. *Physical Review C*, **54**(6): 2986-2995.
10. Caurier, E. and Navratil, P. **2006**. Proton radii of 4, 6, 8He isotopes from high-precision nucleon-nucleon interactions. *Physical Review C*, **73** (021302(R)): 1-5.
11. Karataglidis, S., Amos, K., Fraser, P., Canton, L. and Svenne, J. P. **2008**. Constraints on the spectra of17, 19C. *Nuclear Physics A*, **813:** pp. 235-251.
12. Navratil, P. and Barrett, B. R. **1998**. Large - basis shell-model calculations for p-shell. *Physical Review C* (Nuclear Physics), **57**(6): 3119-3128
13. Adel K. Hamoudi, Raad A. Radhi, Arkan R. Ridha. **2012**. Theoretical study of matter density distribution and elastic electron scattering form factors for the neutron-rich ^{22}C exotic nucleus**.** *Iraqi Journal of Physics*, **10**: *25-34*.
14. Radhi R. A., Hamoudi A. K. and Ridha A. R.**2013**. Elastic Electron Scattering From Unstable Neutron-Rich ^{19}C Exotic Nucleus. *Iraqi Journal of Physics*,**54**: 324-332
15. Hamoudi A. K., Radhi R. A., Ridha A. R. **2015**. Elastic electron scattering from 17Ne and 27P exotic nuclei, *Iraqi Journal of Physics*, **13**(28): 68-81
16. Arkan R. Ridha, Mustafa K. Suhayeb.**2017**. Theoretical Study of Nuclear Density Distributions and Elastic Electron Scattering form Factors for Some Halo Nuclei, *Iraqi Journal of Physics*, **58**: 2098-2106.
17. Saja H. Mohammed , Arkan R. Ridha. **2018**. Theoretical Study of The Electromagnetic Structure of Boron Isotopes Using Local Scale Transformation Technique, I*raqi Journal of Science* , **59**: 1866-1877.
18. Saja H. Mohammed .**2018** .Study of nuclear structure for carbon isotopes using local scale transformation technique in shell model, *Iraqi Journal of Physics*, **16**: 103-116.
19. Arkan R. Ridha and Zaid M. Abbas. **2018**. Study of matter density distributions, elastic charge form factors and size radii for halo ^{11}Be, ^{19}C and ^{11}Li nuclei, *Iraqi Journal of Physics*, **59**: 1046-1056.
20. Arkan R. Ridha. **2016** .Study of charge density distributions, elastic charge form factors and root-mean square radii for 4He, ^{12}C and ^{16}O nuclei using Woods- Saxon and harmonic- oscillator potentials, *Iraqi Journal of Physics*, **14:** 42-50.
21. Arkan R. Ridha, Zaid M. Abbas. **2018**. Theoretical Study of Density Distributions and Size Radii of 8B and ^{17}Ne. *Iraqi Journal of Physics*, **59**: 1046-1056.
22. Arkan R. Ridha.**2017**. Study of Charge Density Distributions and Elastic Charge Form Factors for ^{40}Ca and ^{48}Ca. Journal of Al-Nahrain University, **20**(3): 83-90**.**

23. Ring, P. and Schuck, P. **1981**. *The Nuclear Many-Body Problem*. Springer-Verlag.
24. Elton L. R. B. **1961.** "*Nuclear Sizes*", Oxford University Press.
25. Chandra, H. And Sauer, G. **1976.** Relativistic corrections to the elastic electron scattering from 208Pb. *Phys. Rev. C*, **13**: 245-252.
26. Deforest T., Jr. and Walecka J. D. **1966**. Electron scattering and nuclear structure. *Advances inPhysics*, **15**(57): 1-109.
27. Brown B. A., Wildenthal B. H., Williamson C. F., Rad F. N., Kowisik S. i, crannell H. and O'Brien J. T. **1985**. *Phys. Rev*. **C 32**: 1127-1145.
28. Bohr, A. and Mottelson**,** B.R. **1998.** "*Nuclear Structure Vol II*", World Scientific.
29. Cohen S., Kurath D.**1965**. Nucl. Phys. 73, pp: 1- and Cohen S., Kurath D.**1967**. Nucl.Phys. 101, pp: 1
30. Brown B.A. **2006.** *Phys. Rev. C* **74**, 034315.
31. Brown B.A., Etchegoyen A., Rae W.D.M. **1986.** Computer code OXBASH, MSU Cyclotron Laboratory Report No.524.
32. Chandel, S. S., Dhiman, S. K. and Shyam, R. **2003.** "Structure of 8B and astrophysical S17 factor in Skyrme Hartree-Fock theory". *Phys. Rev.* **C68**: 054320.
33. Blank, B., Marchand, C., Pravikoff, M. S., Baumann, T., Bou, F., Geissel, H., Hellström, M., Iwasa, N., Schwab, W., Sammerer, K. and Gai, M. **1997**. Total interaction and proton-removal cross-section measurements for the proton-rich isotopes 7Be, 8B, and 9C. *Nucl. Phys.* A**, 624**: 242-256.
34. Zhang H.Y., Shen W.Q., Ren Z.Z., Ma Y.G., Jiang W.Z., Zhu Z.Y., Cai X.Z. , Fang D.Q., Zhong C. , Yu L.P., Wei Y.B.,W.L. Zhan b, Z.Y. Guob, G.Q. Xiao b, J.S. Wangb, J.C. Wangb, Q.J. Wang , J.X. Li, M. Wang, Z.Q. Chen. **2002**. Measurement of reaction cross section for proton-rich nuclei (A<30) at intermediate energies . *Nuclear Physics*, **A707**: 303–324.
35. Angeli, I. and Marinova, K. P. **2013**. Table of experimental nuclear ground state charge radii: An update. *Atomic Data and Nuclear Data Tables*, **99**: 69-95.
36. Riisager, K. **2013**. Halos and related structures. *Phys. Scr*. T **152**: 014001.
37. Audi, G., Kondev, F.G., Meng Wang, Huang, W.J., and Naimi, S. **2017**. The NUBASE2016 evaluation of nuclear properties. *Chinese, Physics C,* **41** (030001): 1-138.
38. Takechi, M. , Fukuda, M., Mihara, M., Chinda, T., Matsumasa, T., Matsubara, H., Nakashima, Y., Matsuta, K., Minamisono, T., Koyama, R., Shinosaki, W. , Takahashi, M., Takizawa, A., Ohtsubo, T., Suzuki, T., Izumikawa, T., Momota, S., Tanaka, K., Suda, T., Sasaki, M., Sato, S.and Kitagawa**,** A. **2005**. Reaction cross-sections for stable nuclei and nucleon density distribution of proton drip-line nucleus 8B. *Eur. Phys. J. A***, 25**: 217-219.
39. Tanaka, K., Fukuda, M., Mihara, M., Takechi, M., Chinda, T., Sumikama, T., Kudo, S., Matsuta, K., Minamisono, T., Suzuki, T., Ohtubo, T., Izumikawa, T., Momota, S., Yamaguchi, T., Onishi,T., Ozawa, A., Tanihata, I. and Tao, Z. **2005** . Nucleon density distribution of proton-drip nucleus 17Ne". *Eur. Phys. J. A***, 25**:221-
222.
40. Cichocki, A., Dubach, J., Hicks, R. S., Peterson, G. A., De Jager, C. W., De Vries, H., Kalantar-Nayestanaki, N. and Sato, T. **1995.** Electron scattering from 10B. *Physical Review C,* 51: 2406-2426.
41. Stovall, T., Goldemberg, J. and Isabelle, D. B. **1966.** Coulomb form factors of 10B and 11B. *Nuclear Physics A*, **86**: 225-240.
42. B. A. Brown, B.A. shell –model analysis of high-resolution data for elastic and inelastic electron scattering on ^{19}F. *Phys. Rev*. **C 32**: 1127-1145.
43. E. A. Knight, R. P. Singhal, R. G. Arthur, and M. W. S. Macauley. **1981**. Elastic scattering of electrons from 20,22Ne. *Journal of Physics G (Nuclear Physics)*, **7**: 1115-1121.
44. Dally, E.B., Croissiaux, M.G. and Schweitz, B. *phys. Rev. C2* **1970.** 2057.
45. Knight, E.A., Singhal, R.P., Arthur, R.G. and Macauley, M.W.S**. 1981.** *Phys. G: Nucl. Phys*. 7 (1981) 1115.